Power Electronic Systems
Laboratory

Proceedings of the 33rd Applied Power Electronics Conference and Exposition (APEC 2018),
San Antonio, TX, USA, March 4-8, 2018

Minimum Loss Operation of High-Frequency Inductors

P. Papamanolis,
F. Krismer,
J. W. Kolar

Eidgenössische Technische Hochschule Zürich
Swiss Federal Institute of Technology Zurich

Minimum Loss Operation of High-Frequency Inductors

Panteleimon Papamanolis, Florian Krismer, and Johann W. Kolar

Power Electronic Systems Laboratory (PES)
ETH Zurich, Physikstrasse 3
8092 Zurich, Switzerland
Email: papamanolis@lem.ee.ethz.ch

***Abstract*—This paper investigates the losses of a power inductor employed in a 2 kW, 400 V input DC–DC converter, in dependency of key operating parameters, i.e. switching frequency and current ripple. Based on detailed high-frequency winding and core loss models, including the implications of DC-bias, temperature and frequency on the core losses, and an analytic thermal model, a minimum loss inductor is designed for each combination of switching frequency, f, and current ripple, r. In the course of the optimization, the core (E55, N87) and the winding (litz wire, 100 µm) are considered given. Surprisingly, the evaluation of the losses calculated in the f - r domain reveals that nearly minimum inductor losses are obtained for a current ripple that is inversely proportional to the frequency, i.e., for a constant inductance. Further detailed investigations of the calculated inductor losses reveal a decrease of the losses for increasing frequencies up to a very high frequency of 500 kHz. In this regard, at f = 100 kHz, minimum total losses of 4.0 W result for r = 45 %, which can be reduced to 1.8 W at f = 500 kHz for r = 10 %. Finally, the sensitivities of the losses with regard to different litz wires (71 µm, 200 µm) and a different core (E42, N87) are examined and a design guidance is extracted that summarizes the main findings of the detailed investigation. A calorimetric measurement set-up is used to measure the losses of a realized inductor at different operating points in order to confirm the theoretical considerations.**

I. Introduction

Wide bandgap power semiconductors feature unprecedentedly low switching losses and, due to this, facilitate the use of comparably high switching frequencies for high efficiency power converters with rated power levels of several kW [1]. Accordingly, inductive components with smaller volumes are expected to become feasible, for example, with regard to EMI filters that comply with CISPR 11, for switching frequencies, f, greater than 400 kHz [2]. Hence, recent scientific publications, in particular with regard to GaN power semiconductors, show a trend towards soft-switching converters operated with switching frequencies in the MHz range, where inductors with small inductance values and large current ripples are used to achieve soft-switching (e.g. critical mode or Triangular Current Mode, TCM) [3], [4]. State-of-the-art commercial converters in this power range, however, are often found to operate with $f < 150$ kHz (e.g. 140 kHz), hard-switching, and comparably small inductor current ripples, since, besides switching losses, also further aspects, including the increased implementation effort linked to measurement and control (e.g. resolution of PWM) and additional core and high-frequency (HF) losses in magnetic components, affect decisions in the course of the design process. In particular with regard to filter inductors with magnetic cores, used in buck, boost, and inverter topologies, the prospective reductions of losses and / or component volumes at very high switching frequencies are unclear. On the one hand, the inductor current ripple steadily decreases for increasing switching frequency, if the inductance remains constant. Thus, from a designer's point of view, the resistive losses due to relatively large DC and / or low frequency (LF) current components are expected to become more and more dominant. On the other hand, however, exceedingly high core and HF losses result at very high switching frequencies, even with the RMS value of the inductor current ripple being much less than the DC or LF inductor current.

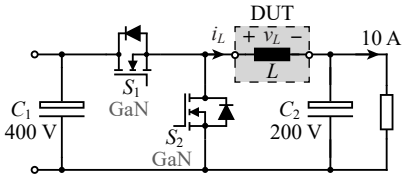

Fig. 1. Buck converter considered for the loss calculation.

Literature reveals that optimal switching frequencies, with regard to maximum power density, exist for inductors of resonant circuits and High-Frequency (HF) transformers [5] and the performance factor, $PF = B_{\mathrm{pk}} f$, (or, to better account for HF losses in the windings, the modified performance factor, $PF_{\mathrm{w}} = B_{\mathrm{pk}} f_{\mathrm{w}}$) has been introduced to directly identify ranges of most effective operating frequencies for magnetic cores [6]. An intuitive extension of the performance factor to inductors of DC–DC converters is proposed in [7]. For the designer of a filter inductor, however, it is not clear whether existing proposals for performance factors denote reasonable guidelines with regard to the inductor's optimal operating conditions, since unconsidered effects may have decisive implications on the losses, e.g., fringing fields of air gaps (HF copper losses), DC bias (core losses), temperature dependencies, etc.

In an alternative approach, the optimal design of a filter inductor may be identified in the course of comprehensive multi-objective converter optimization, e.g., with respect to power density and / or efficiency of the complete power converter. The obtained results, however, often reveal completely different design parameters for similar power densities and efficiencies [4]. As a consequence, it is not possible to extract

TABLE I
CONVERTER SPECIFICATIONS

Input voltage, V_{in}	400 V
Output voltage, V_{out}	200 V
Output power, P_{out}	2 kW
Considered frequencies, f	50 kHz < f < 1 MHz
Core	E55/28/21, N87
Conductor	HF litz wire, single strand diameter of 100 µm
Ambient temperature	55°C

clear guidelines with regard to the selection of suitable converter design parameters in order to enable optimal, e.g. minimum loss, operation of the inductor.

The aims of this paper are to clarify up to which switching frequency a decrease of the inductor losses is achievable; to characterize the reasonable range of operation and identify important influencing parameters, and to verify analytical considerations by means of experimental results. For the sake of clarity, the presented analysis investigates a reduced design space that consists of the two most important design parameters – *switching frequency*, f, and *current ripple*, r – for the DC–DC buck converter specified in **Tab. I** and depicted in **Fig. 1.** The study employs the electromagnetic-thermal (EMT) coupled inductor model summarized in **Section II** to calculate achievable losses of different inductors, that utilize same magnetic cores (E55/28/21, ferrite material N87, no distributed air gaps) in order to eliminate further influences that arise from different core sizes and shapes. The conductor used for the winding is a HF litz wire with single strand diameter of 100 µm. **Section III** identifies characteristic properties of the calculated losses and **Section IV** presents a practical guidance on how to select reasonable operating ranges for a filter inductor with defined core and conductor at a very early stage of converter design, i.e., without taking the complex interactions of non-linear core losses, HF copper losses, and thermal couplings in inductors into account. **Section V** verifies the theoretical findings by means of experimental loss measurements obtained from a calorimetric measurement setup. The measurements reveal 3.7 W at f = 200 kHz and 2.5 W at f = 500 kHz and thus, confirm the decreasing losses for increasing frequency, which is theoretically predicted in Section III.

II. INDUCTOR MODELING

For the evaluation of the inductor, a coupled EMT model is implemented in MATLAB. The coupling is done in an iterative manner until loss and temperature values converge. The core losses are calculated with the improved Generalized Steinmetz Equation (iGSE). The Steinmetz coefficients are obtained by means of interpolation, from pre-measured and tabulated values, which take the implications of flux DC bias, flux AC amplitude, frequency, and temperature into account. The existing values reach up to 270 kHz, above this point the losses are scaled using datasheet values. The AC winding losses in the HF litz wire are calculated according to [8] and the magnetic field in the core window, needed to estimate proximity losses, is determined using the mirroring method [9]. A detailed reluctance model is used to obtain a precise value of the required air-gap and consequently the flux DC bias [10]. The thermal model is based on [11] and improved according to [12].

Due to the high complexity of the investigated inductor model, sinusoidal AC excitation has been considered in order to further simplify the analysis. Sinusoidal and triangular AC excitations consider same peak values according to the given current ripple, cf. **Fig. 2(a)**.

III. EVALUATION AND LOSS CHARACTERISTICS

According to derivations based on scaling laws [13],

$$P_L \propto V_L^{\frac{4(2-\beta)}{3(2+\beta)}-\frac{1}{3}} f^{\frac{2\alpha-2\beta}{2+\beta}} I_{\text{rms}}^{\frac{2\beta}{2+\beta}} U^{\frac{2\beta}{2+\beta}}, \tag{1}$$

which, for $\alpha = 1$ and $\beta = 2$, can be reduced to

$$P_L \propto \frac{U I_{\text{rms}}}{\sqrt{f} V_L^{\frac{1}{3}}}, \tag{2}$$

the minimum achievable inductor losses are expected to be proportional to $1/\sqrt{f}$. However, this derivation does not include the implications of non-linear core losses, HF copper losses, and temperature dependencies of the copper and core losses. Thus, the detailed model of Section II is used to more accurately characterize the losses that result with the considered E55/28/21 core (using ferrite material N87), within wide ranges of frequency and current ripple,

$$50\,\text{kHz} \le f \le 1\,\text{MHz} \quad \text{and} \quad 2\,\% < r < 200\,\%, \text{ with} \tag{3}$$

$$r = I_{\text{AC,pk,pk}} / I_{\text{DC}}, \tag{4}$$

where I_{DC} and $I_{\text{AC,pk,pk}}$ denote DC current and peak-to-peak inductor AC current component, respectively.

At each operating point defined by f and r, the inductance is given with $L = (1-D)DV_{\text{out}}/(f\,r\,I_{\text{DC}})$. Besides the core also a defined conductor, i.e., HF litz wire with single strand diameter of 100 µm is considered. Thus, for given f and r, the only remaining degree of freedom for the optimization of the inductor losses is the number of turns, N. **Fig. 2** depicts air-gap lengths, flux densities, and losses of inductors for considerably different operating points OP_1 (f = 80 kHz, r = 85 %) and OP_2 (f = 500 kHz, r = 8 %), evaluated within $15 \le N \le 38$, to enable the characterization of the results with regard to similarities and differences.

Due to constant inductances (147 µH at OP_1 and 250 µH at OP_2), the air-gap lengths at both operating points increase with increasing N and eventually reach unreasonably high values (> 20 % of core height). AC and peak flux densities increase with decreasing N and thus, core losses decrease with increasing N. Below a certain minimum number of turns the peak flux densities exceed the saturation flux density, B_{sat} (there, the depicted core losses are obtained by means of extrapolation). Furthermore, the current density in the coil is proportional to N and, due to $P_{\text{Cu}} = Vol_{\text{Cu}} J^2/\sigma$ and

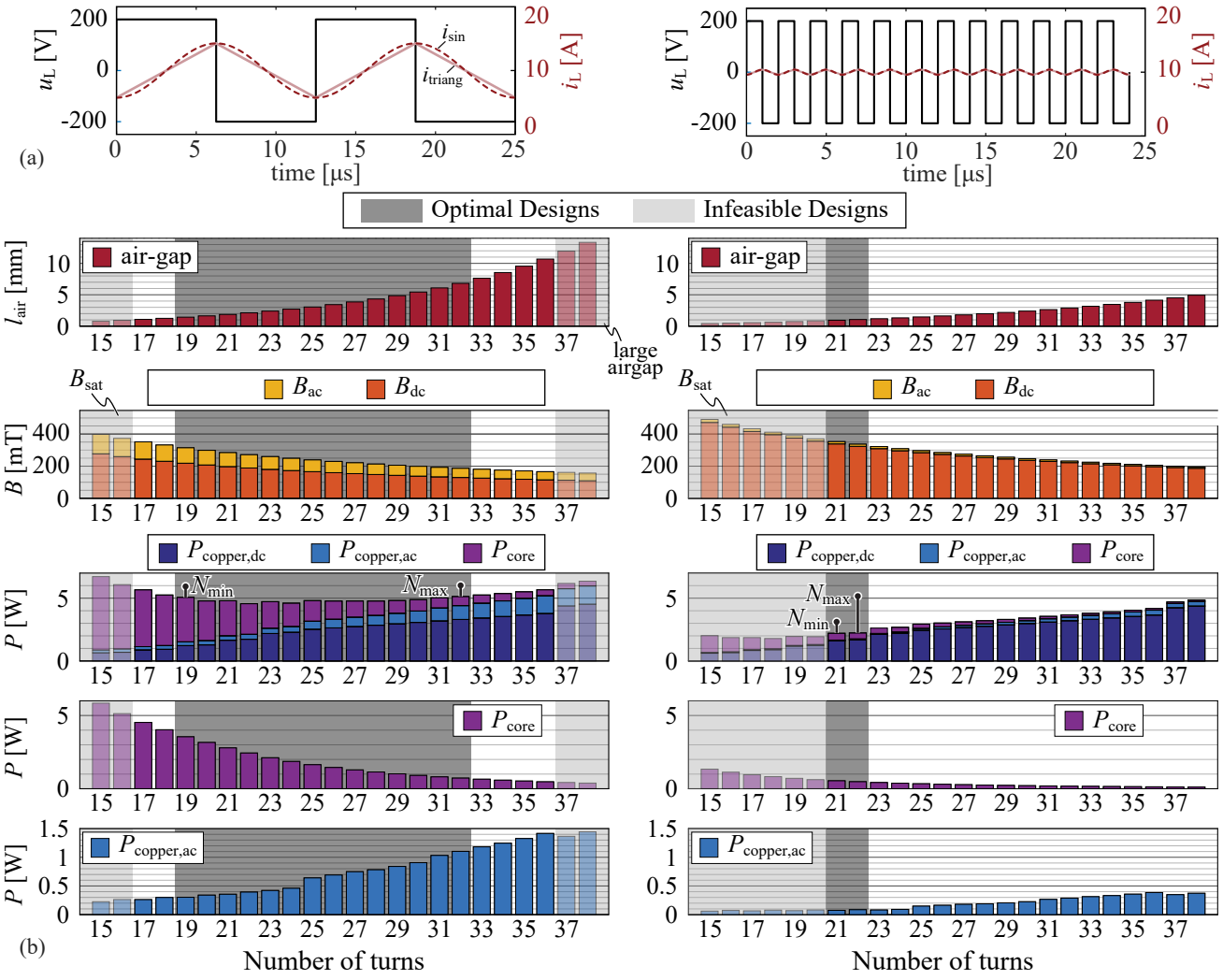

Fig. 2. For two different operating conditions: (left) $f = 80\,\text{kHz}$, $r = 85\,\%$, (right) $f = 500\,\text{kHz}$, $r = 8\,\%$, (a) the voltage and current waveforms of the buck-converter are shown, and (b) the loss-analysis for a broad range of different number of turns is given.

constant copper volume Vol_{Cu}, the total copper losses are proportional to N^2 (J denotes the current density). Fig. 2(b) approximately reflects this result for the copper losses and the two considered operating points, where the imperfections observed in the corresponding bar plots originate from the automatic conductor placement algorithm, which considers rectangular packing and cannot completely fill the outermost winding layer for all values of N. Due to this, the inductor model returns similar losses for 14 different values of N, $19 \le N \le 32$, at OP_1 (the threshold for automatically detecting N_{min} and N_{max} for similar total losses is set to 115 % of the minimum total losses determined for given f and r).

In accordance to (1) and (2), Fig. 2 reveals that substantial loss reductions are achievable at high frequencies, since the impact of a reduced AC flux density on the core losses potentially outweighs the loss increases due to increased frequency. However, at OP_2, minimum total losses would result at $N = 18$ and the magnetic core would saturate. For this reason, only two different designs with $21 \le N \le 22$ remain at 500 kHz.

The inductor design procedure determines the ranges of N that feature low inductor losses for each given operating point in the f-r-plane. Except for the total losses and the temperature, all examined properties, e.g., core and copper losses, air-gap lengths, etc., are evaluated for

$$N(f,r) = \left\lceil \frac{N_{\text{min}}(f,r) + N_{\text{max}}(f,r)}{2} \right\rceil. \tag{5}$$

The depicted total losses and the hot spot temperature, both correspond to the optimal number of turns for each operating point, which results in reduced noise due to the flat behavior of the total losses for $N_{\text{min}} \le N \le N_{\text{max}}$.

Fig. 3 depicts the calculated total losses, copper losses, and core losses with respect to frequency and current ripple. **Fig. 4** depicts the hot-spot temperatures inside the coil, which remain below 110°C for designs located along $r_a(f)$

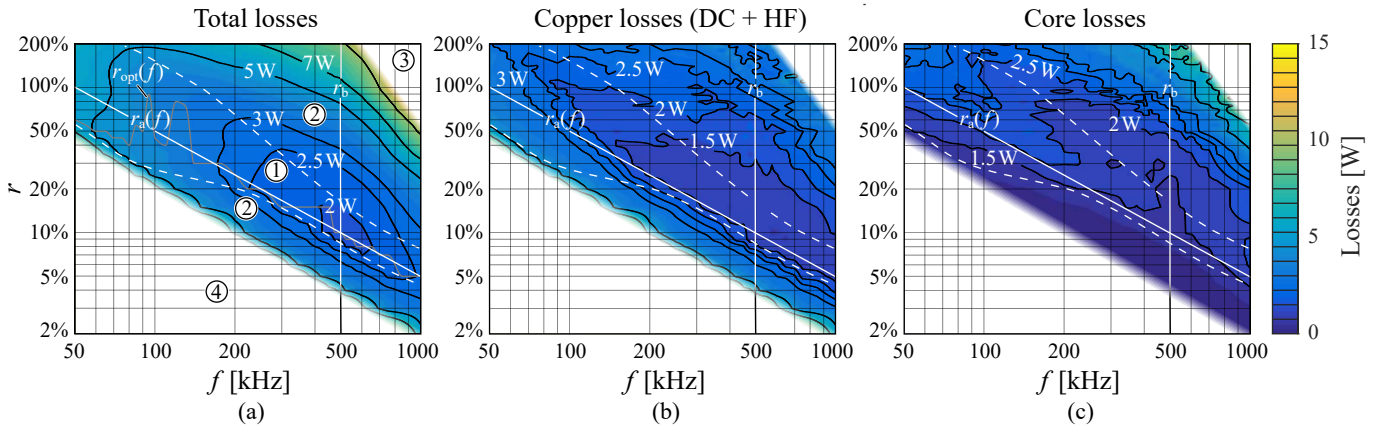

Fig. 3. Calculated inductor losses for a given E55/28/21 core (ferrite, N87) and HF litz wire with single strand diameter of 100 µm: (a) total losses, (b) DC and HF copper losses, and (c) core losses. Each point of the depicted plots corresponds to the result obtained for a locally optimized inductor design, which uses the loss-optimal number of turns. The trajectory $r_{\mathrm{opt}}(f)$ identifies the optimal ripple with respect to minimum losses for given frequency.

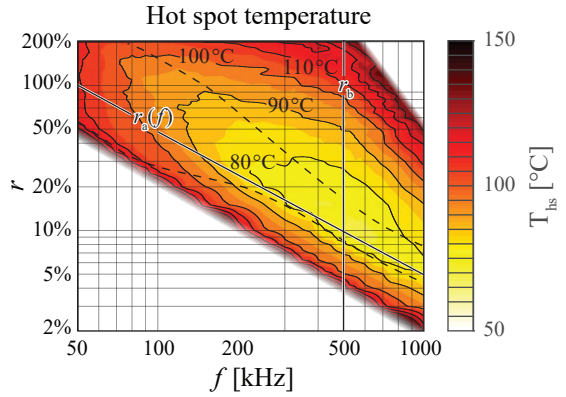

Fig. 4. Hot-spot temperature inside the coil determined with respect to f and r and for a limiting value of 155°C.

and reveals contour lines similar to those of the total losses depicted in Fig. 3(a).

In the course of a close inspection of Fig. 3, four characteristic regions, ① to ④, can be distinguished.

- The two dashed white lines delimit region ①, which denotes ranges of current ripples that facilitate low inductor losses, close to the minimum feasible inductor losses obtained along $r_{\mathrm{opt}}(f)$. The threshold for creating the dashed white lines has been set to 1.15 times the minimum inductor losses calculated for a given frequency. In this context, ① denotes most reasonable ranges of f and r.
- The two regions ② characterize combinations of f and r that facilitate thermally valid inductor designs, however, lead to inductor losses that exceed the threshold specified for region ①.
- Regions ③ and ④ denote combinations of f and r that lead to infeasible inductor designs, which exceed the maximum specified hot-spot temperature of 155 °C. With regard to ③, the reasons are high core and HF copper losses, due to high flux and current ripples at high frequencies. Region ④ requires high inductance values to achieve very low current ripples. Hence, operation close to core saturation, large air-gap lengths, high numbers of turns, and high DC resistances result.

With regard to frequency, feasible minimum inductor losses decrease from 7 W at low frequencies and large ripples, e.g., $f = 70\,\mathrm{kHz}$ and $r = 100\,\%$, to less than 2 W at the global minimum at $f = 500\,\mathrm{kHz}$ and $r = 10\,\%$. According to this result, the chosen magnetic material enables operation above 500 kHz, however, no further decrease of losses is expected above this frequency. Furthermore, it is interesting to see that, for given frequencies, nearly minimum inductor losses are obtained for the trajectory r_{a} delineated in Fig. 3,

$$r_{\mathrm{a}}(f) = \frac{50 \times 10^3}{f/1\,\mathrm{Hz}}, \tag{6}$$

i.e., for a constant inductance.

Fig. 5 depicts losses and characteristic inductor data, evaluated along $r_{\mathrm{a}}(f)$. According to previous results, decreasing losses result for increasing frequency, by reason of decreasing core losses. This can be investigated based on the Steinmetz equation,

$$P_{\mathrm{core}} \propto f^{\alpha} B_{\mathrm{pk,HF}}^{\beta} \propto f^{\alpha} \left(\frac{1}{Nf}\right)^{\beta} \propto f^{\alpha-\beta} N^{-\beta}. \tag{7}$$

Thus, for $\alpha < \beta$, the core losses decrease for increased frequencies and increase for decreased N. Furthermore, for constant inductance, the HF copper losses are approximately independent of the frequency,

$$P_{\mathrm{cu,HF}} \propto R_{\mathrm{DC}} \underbrace{G_{\mathrm{r}}}_{\propto f^2} \underbrace{H_{\mathrm{pk,HF}}^2}_{\propto f^{-2}}. \tag{8}$$

For this reason, the inductor design procedure reduces the number of turns with increasing frequency of the considered operating point, in order to reduce the copper DC losses and achieve minimum total losses by means of balanced

TABLE II
STEINMETZ COEFFICIENTS α AND β FOR N87 AT SELECTED OPERATING CONDITIONS AND AT 70°C.

f / kHz	B_{ac} / mT	α	β
200	25	2.16	2.56
500	13	2.33	2.23
500	25	2.16	2.23

copper and core losses. In the frequency range 300 kHz < f < 750 kHz, however, no further loss reduction is feasible. A closer inspection of the considered ferrite material reveals $\alpha > \beta$ at 500 kHz and low AC flux amplitudes, listed in **Tab. II**. For this reason, and according to (7), the material cannot feature further loss reductions above 500 kHz. In summary, the considered trajectory $r_a(f)$ is found to achieve effective utilization of the given magnetic core by balancing copper and core losses [Fig. 5(a)] and, at the same time, apply high flux densities close to saturation [Fig. 5(e)]. Due to the dominant DC current component and $J_{rms} = NI_{rms}/(k_{fill}A_w)$ (where A_w corresponds to the surface of the core window), the product of current density and fill factor, both depicted in Fig. 5(f), is approximately proportional to N. The air-gap length is adapted according to N and L and is within 1 mm < l_{air} < 3 mm, cf. Fig. 5(d).

The second trajectory depicted in Fig. 6(a), $r_b(f$ = 500 kHz), is used to explore the sensitivity of the inductor losses with respect to the current ripple. **Fig. 6** illustrates the inductor losses and characteristic inductor data along $r_b(f = 500\,\text{kHz})$. With regard to decreasing values of r and $r < 8\,\%$, the core is found to be operated close to saturation, cf. Fig. 6(e). Since L is inversely proportional to r, the number of turns needs to be increased in order to achieve the required inductance and avoid saturation. Thus, the current density, given in Fig. 6(f), and the DC losses increase and the HF copper losses and the core losses decrease. For increasing current ripple and $r > 20\,\%$, the HF copper losses increase. The copper losses can be reduced by decreasing the number of turns, which, however, causes the core losses to increase. Hence, the design procedure reduces the number of turns for increasing r, cf. Fig. 5(c), such that minimum total inductor losses result, which is achieved for similar copper and core losses, cf. Fig. 5(a). As a consequence of the decrease of N, AC flux density increased and the product $k_{fill}J_{rms}$ increases. It is interesting to note that the calculated core losses are nearly constant for 8 % < r < 20 %. The reason for this characteristic is an interaction between copper and core losses: for increasing r the inductance L decreases. Based on the assumption of constant N a decrease of the DC flux density would result, due to an increase of the air-gap length. By reason of the reduced DC flux and unchanged peak AC flux, reduced core losses would result, however, the HF copper losses would increase. As a consequence, the optimization procedure slightly reduces N, which balances copper and core losses, minimizes the total losses, and leads to approximately constant losses in a considerably wide range of r.

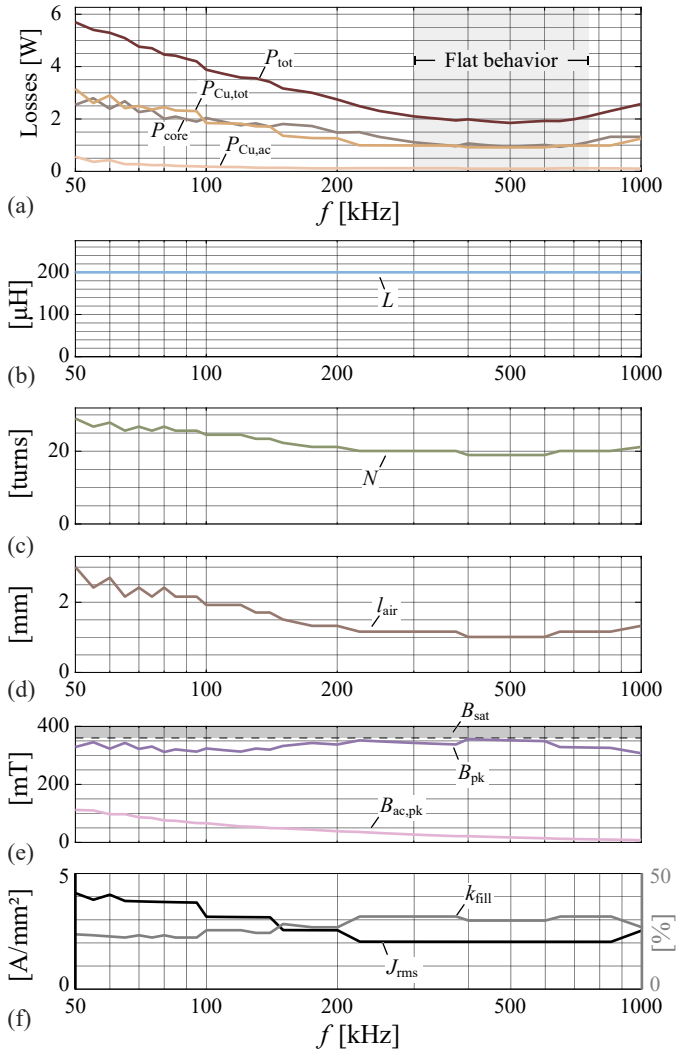

Fig. 5. Design and performance analysis of the optimal designs, along the $r_a(f)$ trajectory depicted in **Fig. 3(c)**.

Fig. 7 illustrates the impact of the selected single strand diameter, d_s, of the HF litz wire on the total inductor losses. Decreased single strand diameters facilitate a reduction of the HF copper losses, which yields a reduction of the total inductor losses at operating points with high frequencies and / or high current ripples. As a result, a decrease of d_s shifts the thermal limit between regions ② and ③ in Fig. 3 toward higher ripples and frequencies and vice versa. The thermal limit between regions ② and ④ is nearly not affected, since it is primarily defined by DC copper losses.

With regard to Fig. 5(d), comparably low air-gap lengths close to 1 mm result for $f > 200$ kHz, which indicates that the selected core could be replaced by a smaller core in order to achieve increased power density. In this context, **Fig. 8** presents the calculated losses for the next smaller E-core E42/21/20 and HF litz wire with $d_s = 100\,\mu$m. The resulting loss characteristic is comparable to that of the

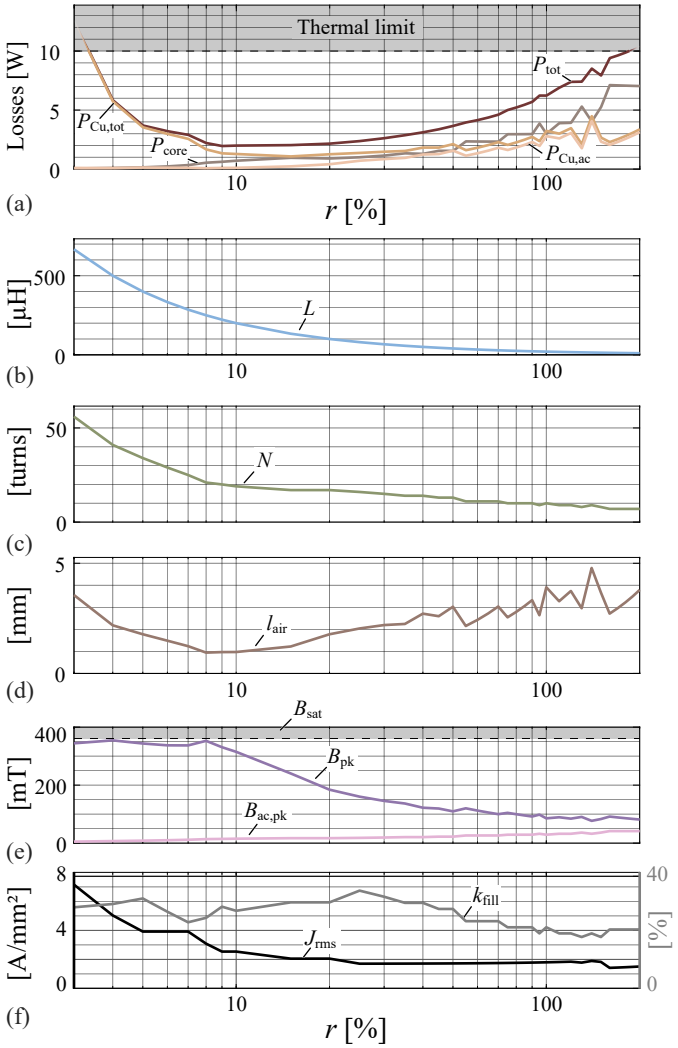

Fig. 6. Design and performance analysis of the optimal designs, along the $r_b(f = 500\,\text{kHz})$ trajectory depicted in **Fig. 3(c)**.

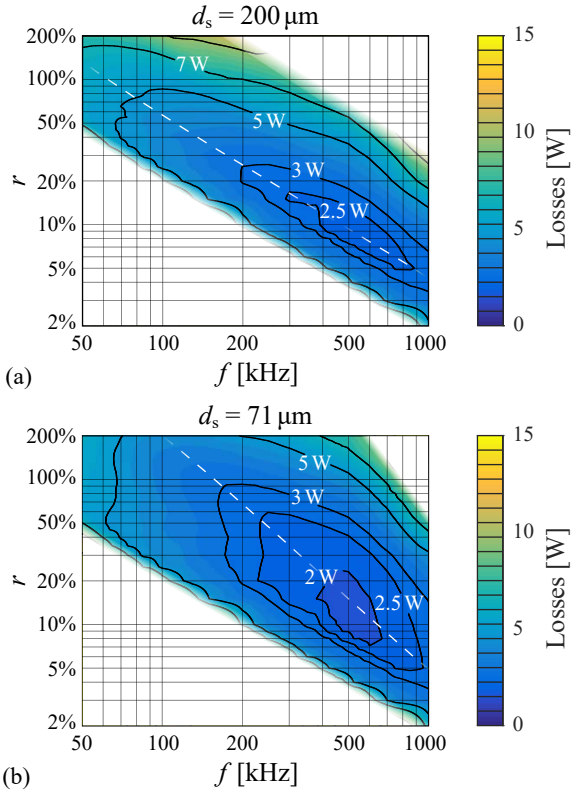

Fig. 7. Calculated inductor losses for inductor designs that employ a given E55/28/21 core (ferrite, N87), optimal number of turns and HF litz wires with different single strand diameters: (a) $d_s = 0.2\,\text{mm}$ and (b) $d_s = 0.071\,\text{mm}$.

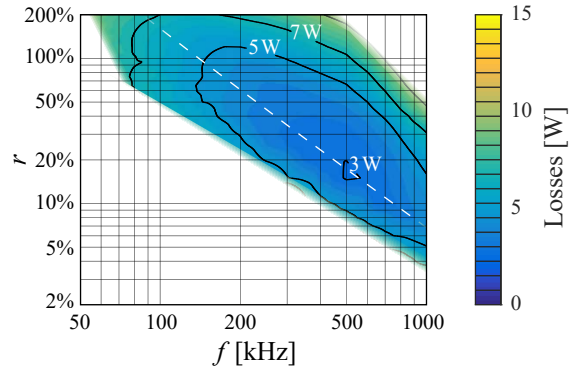

Fig. 8. Calculated inductor losses for inductor designs that employ a smaller core, E42/21/20 (ferrite, N87), optimal number of turns and HF litz wires with a single strand diameter of 100 µm.

E55/28/21 core depicted in Fig. 3, however, the region of minimum losses is shifted towards higher current ripple. In this regard, the global minimum results for $f = 500\,\text{kHz}$ and $r = 20\,\%$ instead of 10 %. Due to complex interactions this behavior is subject to further investigations. Furthermore, the core is found to be too small to facilitate reasonable operation at low frequencies, close to 50 kHz.

IV. Summary for Design Guidance

Main findings of the detailed investigation presented in Section III are summarized below.

- According to Fig. 5 the optimal current ripple for a given frequency does not fall below a value r_0, which denotes the current ripple that simultaneously enables operation close to saturation and balanced copper and core losses.
- For given frequency and current ripple, i.e., given inductance, the number of turns remains as a degree of freedom and is selected such that approximately balanced core and copper losses are achieved (however, N can be changed within a certain range around this optimum, since $30\,\% < P_{core}/P_{cu,tot} < 70\,\%$ is found to yield similar total losses). Furthermore, a reasonable copper filling factor needs to be aimed for.
- Besides this practical approach, the presented investigation of the detailed inductor model also reveals in Fig. 6 that the current ripple may be increased to values considerably higher than r_0 without substantially increasing the total losses. In the investigated example,

TABLE III
INDUCTOR DESIGN CHARACTERISTICS

Core	E55/28/21, N87
Total air-gap	800 µm (= 400 µm per core leg)
Type of conductor	HF litz wire, 900 × 100 µm
No. of turns	16 (2 layers × 8 turns)
Inductance	167 µH

$r_0 = 8\,\%$ and a reasonable range of $8\,\% < r < 25\,\%$ apply at $f = 500\,\text{kHz}$ in Fig. 6.

- According to the different calculated inductor losses depicted in Fig. 3, Fig. 7, and Fig. 8, almost minimum losses are determined along a trajectory in the f-r-plane that corresponds to constant inductance L.

V. EXPERIMENTAL VERIFICATION

For the experimental verification of the above calculation, a calorimetric setup according to [14] and depicted in **Fig. 9(a)** has been implemented, which consists of two enclosures. The outer enclosure (i.e. an oven[1]) provides a constant reference temperature and the inner enclosure contains temperature sensors, heaters (connected to active cooling systems, heat sinks plus fans, to provide a homogeneous temperature distribution inside the inner enclosure), and the Device Under Test (DUT).

The calorimeter is first started without the DUT being operated and a temperature controller, which uses the heaters as actuators, is responsible for setting the inner enclosure's test temperature to a user-defined level, cf. **Fig. 9(b)** for $0 < t < 3000\,\text{s}$. Subsequently, during steady state, the heaters provide a certain power, P_0, to maintain the reference temperature. Thereafter, at $6500\,\text{s} < t < 11\,000\,\text{s}$, the DUT is operated at the required operating point, generating losses, and the controller decreases the heating power in order to preserve constant temperature inside the inner enclosure. The measurement result is ready when the heating power stabilizes again at a certain value, $P_1 < P_0$, and the losses are obtained from the difference $P_0 - P_1$, e.g. at $t = 11\,000\,\text{s}$ in Fig. 9(b). An assessment of the accuracy reveals that the realized system achieves an absolute accuracy of 0.1 W.

The circuit presented in Fig. 9(a) is used to operate the tested inductors. It is composed of a DC supply that provides the DC current, a linear amplifier that provides AC currents up to very high frequencies exceeding 1 MHz, and filters that decouple the two power sources.

For the experimental verification of the calculated results, a single inductor close to the optimal design has been realized. This inductors features similar losses to the inductors along the trajectory r_a depicted in Fig. 3 for a wide range of frequencies, $200 < f < 750\,\text{kHz}$. **Tab. III** lists the details of this inductors. **Fig. 10** depicts the measured impedance of the inductor and reveals a resonance frequency of 2.5 MHz.

[1]The considered oven controls the temperature to a value that is 5°C higher than the ambient temperature

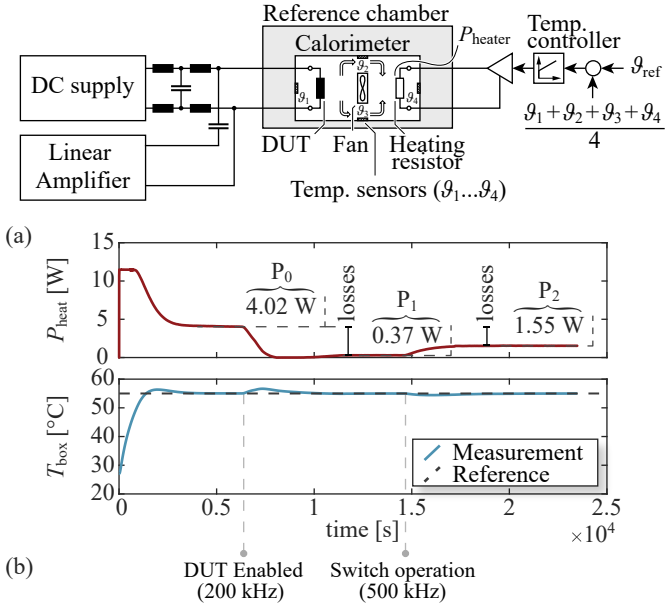

Fig. 9. (a) Schematic of the complete calorimetric setup. (b) Example of a loss measurement procedure.

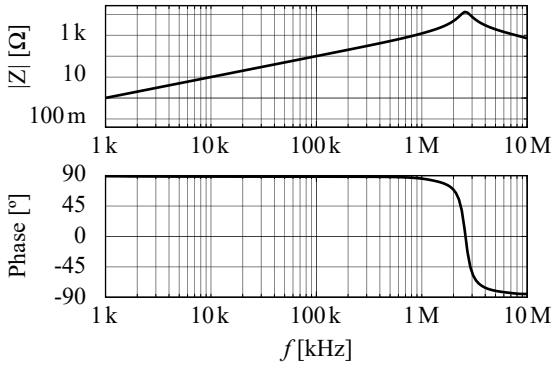

Fig. 10. Measured phase and magnitude of the impedance of the realized inductor. The measurement reveals an inductance of 160 µH and a resonance frequency of 2.5 MHz.

Fig. 11 compares measured to calculated losses. Measured and calculated values follow same trends, nevertheless the calculation underestimates the losses by 0.29 W to 0.56 W. This is to one part attributed to the calculation of the core losses, which, for $f > 270\,\text{kHz}$, are interpolated based on datasheet values. A second source of error are additional AC winding losses due to intense fringing fields close to the air-gap where the considered model is of limited accuracy. The separation of the calculated total losses into the calculated core and copper losses confirms constant copper losses for a given set-up and changing frequency, according to (8). Furthermore, unequal distribution of core and copper losses results at $f = 200\,\text{kHz}$, which, however, causes only a minor deviation of the calculated total losses (3.2 W) from the achievable minimum (2.7 W).

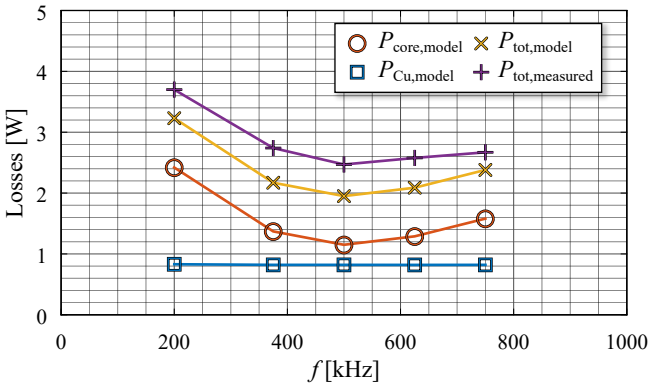

Fig. 11. Comparison between the calculated losses and the losses measured using the calorimetric setup. The inductor presented in Tab. III is operated in 4 different frequencies.

VI. Conclusion

This paper systematically investigates the impacts of switching frequency and current ripple on the losses of loss-optimized power inductors with same E55/28/21 ferrite cores, which are subject to LF and HF currents. In a first step, the commonly used ferrite material N87 is chosen. For the sake of simplicity, a buck converter with constant duty cycle of 50 % is selected and constant input voltage and output DC current are assumed. Furthermore, a sinusoidal instead of triangular ripple is considered. The losses are computed in wide ranges of switching frequency and current ripple with a detailed coupled EMT inductor model, which employs advanced loss models to accurately compute core losses and HF AC losses. According to the obtained result, the minimum inductor losses at the optimal current ripple decrease for increasing switching frequency up to a high frequency of 500 kHz where equal Steinmetz coefficients, $\alpha \approx \beta$, occur. Moreover, low ripple values are found to lead to most efficient inductors at high switching frequencies. Interestingly, the characteristic of minimum inductor losses with respect to frequency and ripple rather corresponds to an almost constant product of ripple and frequency, thus resulting in nearly unchanged inductance value. Furthermore, for the given ferrite core, minimum inductor losses are found at operating points close to a trajectory in the f-r-domain that corresponds to a constant product of ripple and frequency, thus resulting in nearly unchanged inductance value.

These findings are summarized in a design guideline and experimentally verified using a calorimetric measurement setup, which allows testing at user defined ambient temperature. Since it is found that the optimal number of turns remains approximately constant for the given core and frequencies in the range of $200\,\text{kHz} < f < 750\,\text{kHz}$, same optimal inductor design remains. Thus, for the purpose of experimental verification, a close to optimal inductor is built. The measurements reveal 3.7 W at $f = 200\,\text{kHz}$ and 2.5 W at $f = 500\,\text{kHz}$ and thus, confirm the theoretically predicted loss reduction. The presented simplified investigation denotes a first step towards a more comprehensive analysis, which examines inductors with different magnetic cores (sizes, shapes, and materials), types of wires, etc., in order to identify those designs that provide most reasonable compromises between efficiencies and power densities. Moreover, certain converter realizations require a high current ripple, e.g., soft-switching converters using TCM operation with a ripple exceeding 200 %. The analysis of corresponding operating conditions, e.g. varying frequency and constant ripple, are part of future investigations.

References

[1] Z. Liu, B. Li, F. C. Lee, and Q. Li, "Design of CRM AC/DC converter for very high-frequency high-density WBG-based 6.6kW bidirectional on-board battery charger," *Proc. of the IEEE Energy Conversion Congress and Expo. (ECCE USA)*, pp. 1–8, 2016.

[2] J. W. Kolar, F. Krismer, Y. Lobsiger, J. Muhlethaler, T. Nussbaumer, and J. Minibock, "Extreme efficiency power electronics," *Proc. of the International Conf. on Integrated Power Electronics Systems (CIPS)*, pp. 1–22, 2012.

[3] Z. Liu, F. C. Lee, Q. Li, and Y. Yang, "Design of GaN-based MHz totem-pole PFC rectifier," *IEEE Trans. Emerg. Sel. Topics Power Electron.*, vol. 4, no. 3, pp. 799–807, 2016.

[4] J. W. Kolar, D. Bortis, and D. Neumayr, "The ideal switch is not enough," *28th International Symposium on Power Semiconductor Devices and ICs. (ISPSD)*, pp. 15–22, 2016.

[5] W.-J. Gu and R. Liu, "A study of volume and weight vs. frequency for high-frequency transformers," *Proc. of the 24th IEEE Power Electronics Specialists Conf. (PESC)*, pp. 1123–1129, 1993.

[6] "Measurements and performance factor comparisons of magnetic materials at high frequency," *IEEE Trans. Power Electron.*, vol. 31, no. 11, pp. 7909–7924, 2016.

[7] M. S. Rylko, B. J. Lyons, J. G. Hayes, and M. G. Egan, "Revised magnetics performance factors and experimental comparison of high-flux materials for high-current dc–dc inductors," *IEEE Trans. Power Electron.*, vol. 26, no. 8, pp. 2112–2126, 2011.

[8] J. Ferreira, "Analytical computation of AC resistance of round and rectangular litz wire windings," *IEE Proceedings B – Electric Power Applications*, vol. 139, no. 1, p. 21, 1992.

[9] J. Muhlethaler, M. Schweizer, R. Blattmann, J. W. Kolar, and A. Ecklebe, "Optimal design of LCL harmonic filters for three-phase PFC rectifiers," *IEEE Trans. Power Electron.*, vol. 28, no. 7, pp. 3114–3125, 2013.

[10] J. Muhlethaler, J. W. Kolar, and A. Ecklebe, "A novel approach for 3D air gap reluctance calculations," *Proc. of the 8th International Conf. on Power Electronics (ICPE)*, pp. 446–452, 2011.

[11] V. Valchev and A. Van den Bossche, *Inductors and Transformers for Power Electronics*. CRC Press, 2005.

[12] R. Burkart, "Advanced modeling and multi-objective optimization of power electronic converter systems," *Ph.D. dissertation, ETH Zurich*, 2016.

[13] J. Biela and J. W. Kolar, "Pareto-optimal design and performance mapping of telecom rectifier concepts," *Proc. of the Power Conversion and Intelligent Motion Conference, Shanghai, China*, pp. 1–13, 2010.

[14] T. Kleeb, B. Dombert, S. Araújo, and P. Zacharias, "Loss measurement of magnetic components under real application conditions," *Proc. of the European Conf. on Power Electronics and Applications (EPE)*, pp. 1–10, 2013.